AGU PUBLICATIONS

Water Resources Research

RESEARCH ARTICLE
10.1002/2014WR015291

Electrical permittivity and resistivity time lapses of multiphase DNAPLs in a lab test

Luciana Orlando[1] and Beatrice Renzi[1]

[1]Department of Ingegneria Civile, Edile e Ambientale Sapienza University, Rome, Italy

Key Points:
- Mapping and monitoring of separate and dissolved phases of DNAPL
- Joint interpretation of noninvasive surveys of ERT and GPR
- Controlled lab tests in saturated sand

Correspondence to:
L. Orlando,
luciana.orlando@uniroma1.it

Citation:
Orlando, L., and B. Renzi (2015), Electrical permittivity and resistivity time lapses of multiphase DNAPLs in a lab test, *Water Resour. Res.*, *51*, 377–389, doi:10.1002/2014WR015291.

Received 14 JAN 2014
Accepted 7 DEC 2014
Accepted article online 16 DEC 2014
Published online 20 JAN 2015

Abstract Dense Non-Aqueous Phase Liquids (DNAPLs) induce variation in electromagnetic characteristics of the ground, e.g., electric permittivity and resistivity. The most used indirect methods in the mapping of these physical characteristics are electrical resistivity and ground penetrating radar. To better understand the effect of DNAPL release on electrical permittivity and resistivity in a water saturated medium, we carried out a controlled laboratory experiment where the host material was simulated by glass beads and the DNAPL by HFE-7100 (hydrofluoroether). The experiment measured the electric resistivity and permittivity of each fluid, the multiphase fluid system, and the host material, along with time-lapse electrical resistivity and GPR measurements in a controlled cell. We found that the different phases of DNAPL within a saturated medium (free, dissolved, and gaseous phase) affect the physical characteristics differently. The reflection pull-up behind contaminated sediments, which is normally detected by GPR, was mainly inferred from the HFE free phase. The dissolved phase causes small variations in electric permittivity not usually readily detected by GPR measurements. Both the dissolved and free HFE phases induce variation in resistivity. The study showed that GPR and electrical resistivity differ in sensitivity to the different HFE phases, and can be complementary in the characterization of DNAPL contaminated sites.

1. Introduction

In recent years, geophysical methods in the detection and monitoring of contaminants commonly known as Dense Non-Aqueous Phase Liquids (DNAPLs) have become very important in the remediation of contaminated sites. Several studies [*Cardarelli and Di Filippo*, 2009; *Hwang et al*., 2008; *Johnson and Poeter*, 2005; *Goes and Meekes*, 2004; *US EPA (Environmental Protection Agency)*, 2004; *Newmark et al*., 1998; *Daily and Ramirez*, 1995, *Brewster and Annan*, 1994] have shown the effectiveness of geophysical methods in the location and remediation of sites contaminated by DNAPLs. The combination of geophysical data and conventional intrusive data from soil and water sampling [*Chambers et al*., 2010] has the advantage of producing information concerning the entire contaminated area at low cost and in a relatively short time. The scientific community now accepts that a detailed characterization and precise monitoring of the source and location of contamination is essential to a reclamation project [*Kavanaugh et al*., 2003]. However, to date, the potentiality of geophysical data in the assessment of a contaminated site has not been fully exploited; for example, contaminated areas are mapped by geophysical investigations but there is no linking of the geophysical anomalies to the specific phases (free, dissolved, and gaseous) of the contaminant. This is due to the complex interactions between contaminant, sediment, and water [*Abdel et al*., 2006] and to the lack of studies devoted to finding exhaustive answers to such questions.

DNAPLs include chlorinated solvents, compounds derived from hydrocarbons by aliphatic and cyclic hydrocarbons such as tetrachloroethylene (PCE), trichloroethylene (TCE), carbon tetrachloride, etc., all of which dissolve in water to varying degrees, according to their solubility. After release into the environment, DNAPLs migrate by gravity, and because of their high density they tend to move downward through the vadose zone and into the saturated zone, until reaching a low-permeable layer. During the downward movement, part of the DNAPLs remains trapped among the pores of the traversed medium, and this leads to discontinuous bodies (residues). When passing through the water table, part of the DNAPLs still in the free phase dissolves, contaminating the aquifer. Thus, the dissolved phase moves along with the groundwater flow and also contaminates areas far from the point of release, even for a long period of time [*Illangasekare et al*., 1995]; over time, bacteria cause hydrocarbon biodegradation [*Abdel et al*., 2006; *Isalou et al*.,

Table 1. Physical Parameters of the Artificial Porous Media Used in the Experiment

	Porosity (Average) (Measured)	Specific Weight (g/cm^3)	Bulk Density (g/cm^3) (Calculated)	Permittivity (Calculated)
Glass beads (0.4–0.8 mm)	0.388	2.50	1.53	11.20
Glass beads (0.1–0.2 mm)	0.373	2.50	1.57	10.83

1998]. Although the mass transfer process occurring between water and DNAPL is well known, the process that occurs in natural systems under real complex hydrogeological settings continues to be the subject of many studies [*Page et al*., 2007]. Indeed, the distribution of DNAPL is greatly dependent on the permeability and heterogeneity of the traversed porous medium [*Schwille*, 1988; *Kueper and Frind*, 1991], and many studies have been carried out on both the laboratory scale [*Powers et al*., 1998; *Saba and Illangasekare*, 2000] and at the level of theoretical models [*Powers et al*., 1998; *Nambi and Powers*, 2003; *Bradford et al*., 2003; *Parker and Park*, 2004]. In any case, the influence of the medium's heterogeneity on DNAPL migration still remains uncertain [*Fure et al*., 2006], and even a theoretical analysis of the phenomenon is complex as it is difficult to recreate the exact distribution of the DNAPL in the subsurface [*Brusseau et al*., 2007]. In fact, in soil, the DNAPL free phase is not necessarily present as a continuous phase, and the extension of the contaminated area, the result of both free and dissolved phases, is highly dependent on the physical-chemical properties of both the host sediments and the contaminant. Free and dissolved phases can be present in the same area, and their percentages can vary from one point to another. In addition, the width of the transition zone lying between the contaminated and noncontaminated areas depends on the physical characteristics of the host sediments and contaminant.

The achievement of a better understanding of the behavior of DNAPL within a medium requires controlled experiments using geophysical methods that lead to knowledge of the physical parameters of the single phases, fluid mixtures and host material.

In a previous study [*Orlando and Renzi*, 2013], conducted in a controlled cell, we confirmed that DNAPL induces increased electromagnetic wave velocity that is detectable by pull-up of the reflections behind the contaminant, which was also shown by *Bradford et al*. [2003] who analyzed GPR multifold data. Some controlled experiments involving ERT measurements [*Weller et al*., 1996; *Chambers et al*., 2004] demonstrated that DNAPLs increase soil resistivity. For the LNAPLs themselves, *Mazác et al*. [1990] and *Cassidy* [2007] found a decrease in resistivity.

The work presented here continues on from previous work [*Orlando and Renzi*, 2013], extending the observations on measures to include electric resistivity and permittivity of the fluid mixture, and including electric resistive and GPR measurements in a controlled cell over time. The aim was to develop a better understanding of the sensitivity of such geophysical methods to the different phases of DNAPL and not to analyze the complex chemical and biochemical process that occur in the cell over time. The study is focused on pointing out the effectiveness of the integration of more geophysical methods in describing the interaction of the contaminant with a saturated medium and showing that even in a controlled environment, occur complex phenomena that can be explained only with an interdisciplinary approach by involving experts such as chemical, geochemical, biologist, mineralogist, etc.

2. Methodology

The study took into account measures of the electric resistivity and permittivity of the host material and multiphase fluids involved in the cell lab experiment, measurements of electric resistivity and GPR data in the cell, analysis and correlation of data, and the reaching of some conclusions.

The porous medium was simulated by glass beads of two different sizes, i.e., fine, 0.1–0.2 mm, and medium-coarse, 0.4–0.8 mm, with properties specified in Table 1. The DNAPL was simulated by a nontoxic mixture of 96% hydrofluoroether (HFE-7100) and 4% methyl caprylate, properties specified in Table 2. Methyl caprylate is soluble in ether and alcohol, and insoluble in water [*Morris*, 1992].

The chosen dye was Sudan blue (0.22 per 1000 mL), a hydrophobic organic compound that allows the viewing of free phase HFE [*Kamon et al*., 2004].

Table 2. HFE and DNALP Properties

	Fluids		
Properties	*HFE-7100*	*TCE*	*Water*
Relative density (g/cm^3)	1.50	1.464	1.000
Relative viscosity (cP)	0.60	0.59	1.000
Surface tension (mN/m)	13.60	29.30	71.75
Vapor pressure (kPa)	28	7.73	2.34
Solubility in water (mg/L)	12	1100	
Permittivity	10.4[a]	3.35[b]	80
Conductivity (S/m)	10^{-6}	10^{-6c}	5.5×10^{-2a}

[a]Laboratory measurement.
[b]By *Ajo-Franklin et al.* [2004].
[c]By *Olhoeft* [1992].

In any case, the percentages of methyl caprylate and Sudan blue involved in the experiment are so small compared to the percentage of pure HFE that we can advance the hypothesis that they do not significantly influence the physical parameters of the medium.

2.1. Multiphase Fluid Measures

In order to better understand the relation between the physical parameters measured during the experiment, we measured the resistivity (Table 3) and permittivity (Table 2) of each component in the cell: glass beads, water, and HFE mixture, methyl caprylate and Sudan blue. The final mixture was obtained by the release of HFE in the water.

Electric permittivity and resistivity were, respectively, measured with a TDR probe and a portable conductivity meter. The data show the mixtures to be much more sensitive to water permittivity than to HFE, the permittivity of the water-HFE (1%) mixture being very similar to that of water. Indeed, the permittivity of water itself and pure HFE-7100 is little influenced by methyl caprylate and Sudan blue, and their mixtures have a resistivity very similar to that of water. Instead, the resistivity of a mixture (water and HFE-7100) is strongly influenced by HFE-7100; in fact, the resistivity of the mixture contaminated with 1% of HFE is about 4 times the resistivity of uncontaminated water. The measures show that both methyl caprylate and Sudan blue increase water resistivity. As HFE-7100 is present in the mixture to a concentration of 96%, we can be assured that it makes the maximum contribution to the increase in resistivity.

Also mixtures of water/HFE-7100/methyl caprylate/Sudan Blue were measured in different contaminant concentrations over time (Table 4) to check whether any chemical or bacteriological process affects fluid permittivity and resistivity. In fact, *Abdel et al.* [2006] show that in aerobic environments bacteria induce a decrease in fluid resistivity through LNAPL biodegradation. The measurements show that immediately after the HFE mixture is released into the water the permittivity drops to below that of water, but after about 24 h it rises to become equal to that of water again. Resistivity, instead, increases with the release of the HFE mixture, and remains higher than that of water even after several hours. Assuming that HFE migrates quickly downward, its density being higher than that of water, it can be presumed that the measures collected a few seconds after the injection of HFE depend on both water and the HFE free phase. Instead, the measures taken several hours later are influenced only by water and the dissolved phase of the contaminant, the free phase having settled to the bottom. The increase in the resistivity of the fluid after contamination and the small variation in permittivity, which remains very similar to that of water, suggest that the HFE phase dissolved in the water is a nonpolar molecule. Moreover, the free phase of HFE in the saturated medium influences both permittivity and resistivity.

2.2. Cell Setup and Data Acquisition

We designed the experiment with the aim of monitoring the migration of the multiphase fluid over time, through measurements of permittivity, GPR, and electrical resistivity. We also planned to evaluate the effects of water drainage in the removing of DNAPL. For the experiment, we made a cell, 103 cm wide $\times$ 70 cm high $\times$ 19 cm deep (Figure 1a) in plexiglas, which we filled with glass beads (Figure 2). The phreatic surface was maintained constant to collect geophysical measurements in a saturated media. The cell was contaminated with 300 mL of a mixture of HFE-7100.

Table 3. Measurements of Permittivity and Resistivity of Some Fluids

Mixture Composition (T = 20°C)	Permittivity (ε_r)	Resistivity (ρ) (Ωm)
Water	80.11 ÷ 80.78	18
HFE-7100 absolute	10.52 ÷ 10.55	[a]
HFE (96%) + methyl caprilate (4%)	10.48 ÷ 10.61	[a]
Mixture with HFE[b]	10.40 ÷ 10.55	[a]
Water + HFE-7100 (1%)	76.77 ÷ 76.85	72
Water + methyl caprilate	79.38	29
Water + Sudan Blue	80.14	24

[a]Resistivity not measurable/infinite.
[b]HFE-7100 + methyl caprilate + Sudan blue.

We simulated several flows of water over time to monitor the effect on HFE

Table 4. Resistivity and Permittivity Measurements of the Mixture of Water/HFE-7100/Methyl Caprylate/Sudan Blue at Different Concentrations

Fliud	Time[a]	ε	ρ(Ωm)
Water		80.35	18
Water+ Mixture of HFE (1%)	A few seconds	76.07	
Water+ Mixture of HFE (1%)	2 h	76.86	
Water+ Mixture of HFE (1%)	4 h	76.85	
Water+ Mixture of HFE (1%)	4 days	80.20	
Water+ Mixture of HFE (2%)	A few seconds	76.92	
Water+ Mixture of HFE (2%)	24 h	80.40	
Water+ Mixture of HFE (3%)	A few seconds	76.97	72
Water+ Mixture of HFE (3%)	24 h	80.24	78

[a]Time between the entry of HFE in water and permittivity and resistivity measurements.

migration. Flow was simulated by injecting the water at the top right of the cell and draining it off by a tap located on the left side of the cell, 10 cm above the cell bottom. Figure 2a shows the entry and exit points of the water. All the simulated flows were conducted in the saturated cell. We injected water with resistivity equal to that used to saturate the medium at the beginning of the experiment. The details relating to the opening of the flow and the relative flow rates are shown in Table 5. The water was injected using a peristaltic pump and the water flow rate was measured manually, for this reason, the flow rates differ from time to time, from a minimum value of 4.5 to a maximum of 8.2 L/h.

The migration of the contaminant was monitored over 155 days by electrical resistivity, GPR, and permittivity measurements, as described below. The monitored temperature showed a $\pm 1^{\circ}$C variation throughout the experiment.

The resistivity measurements were collected with electrodes inserted in holes (diameter 0.5 cm) drilled at the back of the cell (Figure 1b). Measuring points were located inside the black bordered box of Figure 2a. Electrode distances from the edges of the cell were selected on the basis of theoretical models, which allowed us to define the maximum electrode distances able to reduce border effects on the resistivity measurements.

We used gold plated brass electrodes: diameter 2 mm, pin length 11 mm, contact resistance of 0.4 mΩ. The electrodes were arranged in five lines, placed 7 cm apart in the *x*-direction and 10 cm in the *y*-direction (Figure 1b); the measures were collected only on lines 1–4 of Figure 2b. The first line was positioned at 11.5 cm from the bottom of the cell, and the last one at 11 cm from the top of saturated medium. We made 27 surveys over 155 days (Table 5) with a geo-resistivity meter (Syscal Pro of Iris Instruments) using a dipole-dipole array (see the scheme of Figure 1c), and the measures were referred to the central point of each array.

The GPR data were acquired on the x-y front face of the cell according to the grid mapped in Figure 2a, and the investigated area was larger than that for the electrical resistivity measurements. We used a 2 GHz bipolar antenna, two copolar antennas lying parallel to the profile direction and two perpendicular to it.

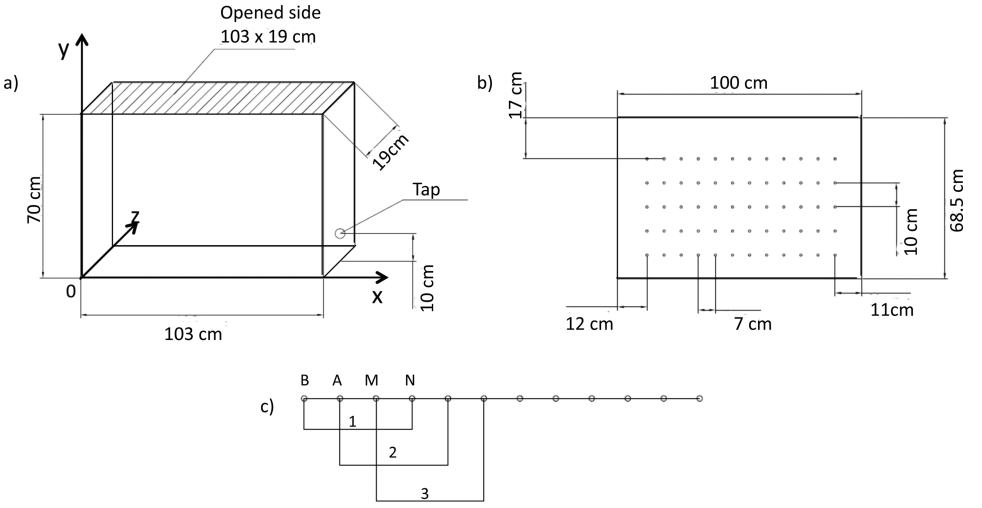

Figure 1. (a) Geometry of the cell, (b) position of holes for the electrodes on the back face of the cell, and (c) resistivity measurement scheme.

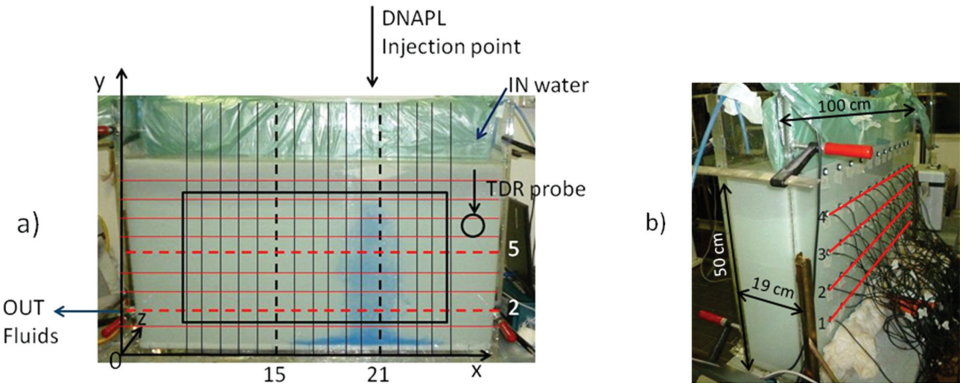

Figure 2. Photos of cell with (a) the grid of GPR profiles and (b) electrode positions. The electrodes are located inside the black box in the left image. The arrow indicates the top of the TDR probe. The ERT data were collected on lines 1–4.

For each survey, we acquired 16 profiles, moving the antenna in the *y*-direction, and nine profiles moving the antenna in the *x*-direction; in both directions, the profiles were spaced 0.05 m apart. The data were acquired with a spatial sampling interval of 0.004 m and with 512 samples per trace.

The GPR surveys were repeated 18 times over time (see Table 5).

Permittivity was measured with a TDR probe positioned at the right side of the cell (Figure 2a), the probe being inserted approximately 20 cm from the top of the saturated sand with the three rods (of the probe) parallel to the x-y plane. Table 5 lists the permittivity measurements collected over time.

The electrical resistivity, GPR, and TDR measurements were collected in the same time.

3. Results and Discussion

At the beginning, the data of each method are analyzed separately, and then interpreted jointly.

Table 5. Description of the Stages of the Water Flow Opening Between the Test Shown in Table 6

Test n	Contents Inside the Cell	Time Post Injection	Electric Measurements	GPR Measurements	TDR Measurements
1	Glass beads/water		X	X	X
2	Glass beads/water/HFE	10 min	X		X
3	Glass beads/water/HFE	30 min	X	X	X
4	Glass beads/water/HFE	50 min	X		
5	Glass beads/water/HFE	1 h	X	X	X
6	Glass beads/water/HFE	2 h 30 min	X	X	X
7	Glass beads/water/HFE	17 h	X		
8	Glass beads/water/HFE	18 h 30 min	X	X	X
9	Glass beads/water/HFE	21 h	X	X	X
10	Glass beads/water/HFE	92 h	X	X	X
11	Glass beads/water/HFE	121 h	X	X	X
12	Glass beads/water/HFE	141 h	X	X	X
13	Glass beads/water/HFE	190 h	X	X	X
14	Glass beads/water/HFE	283 h	X	X	X
15	Glass beads/water/HFE	449 h	X	X	X
16	Glass beads/water/HFE	475 h	X	X	X
17	Glass beads/water/HFE	599 h	X	X	X
18	Glass beads/water/HFE	34 days	X	X	X
19	Glass beads/water/HFE	48 days	X	X	X
20	Glass beads/water/HFE	54 days	X	X	X
21	Glass beads/water/HFE	54 days 5 h	X	X	X
22	Glass beads/water/HFE	60 days	X		
23	Glass beads/water/HFE	60 days 4 h	X		
24	Glass beads/water/HFE	60 days 5 h	X		
25	Glass beads/water/HFE	60 days 6 h	X		
26	Glass beads/water/HFE	61 days	X		
27	Glass beads/water/HFE	155 days	X	X	

Table 6. Description of ERT, GPR, and TDR Measurements[a]

Flow Opening	Time (h)	Flow (L/h)
Between test 15 and 16	8	7.5
After test 16	9	6.5
Before test 19	8	7.2
Between test 20 and 21	5	4.5
Between test 22 and 23	4	8.2

[a]The HFE was injected only once before test 2 for a total volume of 300 mL.

3.1. TDR Measurements

The TDR measurements collected during the experiment provided information about the permittivity variation away from the HFE injection point (Figure 2a). After the release of the contaminant (dotted line on the left of Figure 3), the electric permittivity decreases by about 3.5% of the starting value, but then, with time, it increases. After the water flow (dotted line on the right of Figure 3), the permittivity returns to the same value as before the HFE injection. As the probe lies outside the area of HFE release (Figure 2a), we can assume that it measured water mainly contaminated by the dissolved phase of HFE. Because of the small variation in electrical permittivity before and after HFE release, it can be deduced that the dissolved phase induces small changes in the permittivity of the medium. This is in agreement with the results of electrical permittivity measurements of the fluids described in the multiphase measures (Table 4). This result shows that, probably, in real cases, the dissolved phase of HFE does not induce detectable reduction in the electromagnetic reflection time, in the radargram.

3.2. GPR Data

The GPR data processing was aimed at increasing the signal-noise ratio, and included the repositioning of time zero, the averaging of three traces, background removal and band-pass filtering (300–1600 MHz). To eliminate the effect of the source, the traces of each profile were normalized to the maximum absolute value of its direct wave.

The results of the experiment will be analyzed considering some representative profiles, focusing attention on the two-way travel time (t.w.t) of reflection from the x-y back of the cell opposite the antenna, the most significant attribute for detecting HFE [*Orlando and Renzi*, 2013; *Bano et al*., 2009; *Bradford et al*., 2003]. An earlier experiment [*Orlando and Renzi*, 2013] showed that small HFE volumes, like that in this study, do not generate significant cross-polarized energy. Thus, given the lack of significance of cross-polar data, this paper reports data acquired with copolar antennas in the *x* and *y*-directions.

The main experimental phases, shown for tests 1, 10, 13, 27, of the *x* and *y*-direction profiles can be seen in Figures 4 and 5, which summarize all tests. The profile locations are indicated with dotted lines in Figure 2a. The *x*-direction profiles are labeled with 2 and 5, and the *y*-direction profiles with 15 and 21.

Test 1 (Figures 4a and 5a) monitors the experiment before the release of HFE, and is considered the reference test for the experiment. Tests 10 and 13 (Figures 4b, 4c, 5b, and 5c) monitor the experiment over time before the simulation of water flow, and test 27 (Figures 4d and 5d) monitors the experiment after several occurrences of water flow and the lowering/rising of the water table level. In any case, to avoid wrong considerations related to an incorrect calibration of the data, the analysis is focused mainly on the variation in amplitude of each profile.

In Figures 4 and 5, zero time is the antenna position, and the black arrow (at about 6 ns) indicates the t.w.t. of reflection from the back of the cell. The *x*-direction profiles (Figure 4) cross the cell along the x-z horizontal planes at different distances from the contaminant source (Figure 2a). The source position is projected on the profile and indicated with a black cross. The black circle in Figure 4 indicates the position of the TDR

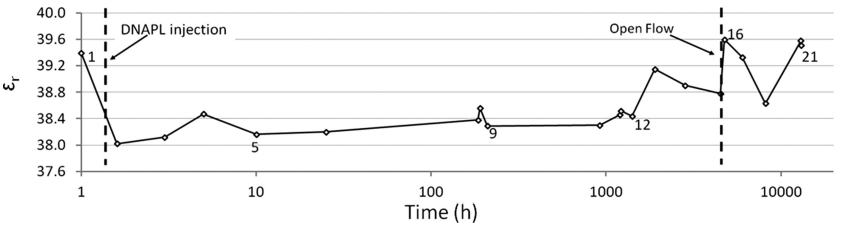

Figure 3. Relative Permittivity versus time. The time is in a logarithmic scale. The dotted line on the left indicates the time injection of HFE, and the one on the right the beginning stages of opening/closing water flows.

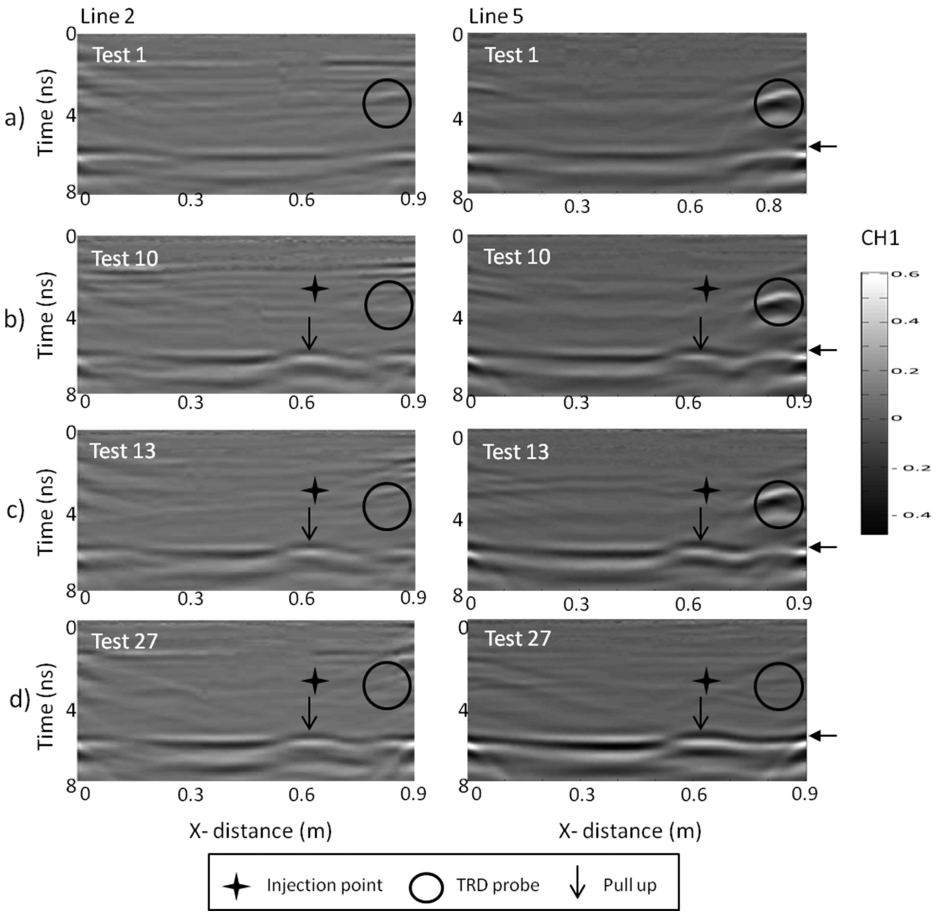

Figure 4. The *x*-direction profiles of lines (left) 2 and (right) 5 of tests (a) 1, (b) 10, (c) 13, and (d) 27. The profile positions in Figure 2a.

probe inside the cell, and the black cross in Figures 4 and 5 indicates the HFE injection point that is in correspondence with the end of line 21. The radargrams show the diffraction from the cell edges and small-scale anomalies due to the inhomogeneity of the host material. Comparing the *x*-direction profiles acquired before and after HFE release (Figures 4a and 4b), we observe a time decrease (pull-up) of the reflected wave from the x-y back face of the cell, in correspondence with the HFE injection point of test 10. This confirms that the contaminant induces an increase in e.m. velocity, as shown by *Bradford et al*. [2003], *Bano et al*. [2009], *Orlando and Renzi* [2013], and many others. The pull-up persists in the *x*-direction profiles over time (Figure 4c) and also after several water flows. After the lowering and rising of the water table level, pull-up persists only in the data acquired in sediments remained saturated during the whole experiment (Figure 4d).

Figure 5 shows two *y*-direction profiles that cross the cell along the y-z planes, as shown in Figure 2a. Line 15 is located to the left of the HFE injection point and line 21 lies along the flow of HFE.

The *y*-direction profiles show an increase in the reflection time from the back of the cell, from the cell bottom to the top, due to cell deformation resulting from horizontal forces applied by the material filling the cell. The maximum deformation of the cell was 1.5 cm, which is consistent with the maximum time variation of 0.5 ns for a measured electromagnetic wave velocity of 5.7 cm/ns. This is easily visible in the data acquired before the release of HFE (Figure 5a).

The line 21, acquired along the flow of HFE and after its release (right of Figure 5b), clearly show a pull-up, at 0.3–0.35m from the cell bottom, of the reflection from the back of the cell, with respect to the data acquired before the release of HFE (right of Figure 5a). Over time the pull-up remains very similar in all the data collected before the water flow simulation (Figures 5b and 5c). Instead line 15, acquired to the left of

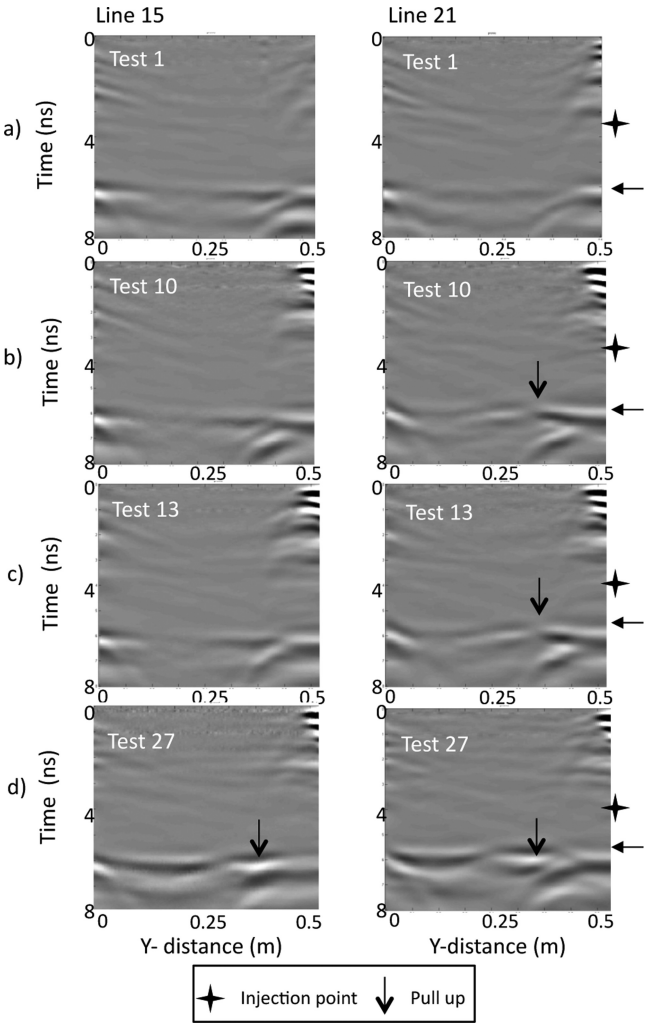

Figure 5. The *y*-direction profiles of lines (left) 15 and (right) 21 of tests (a) 3, (b) 10, (c) 13, and (d) 27. The profile positions in Figure 2a.

the HFE release, do not show any detectable pull-up of the reflection time in the tests collected before the water flow simulation (left in Figures 5b and 5c). All the data collected in the *y*-direction, after the lowering/rising of the water table level, show pull-up in the same position (Figure 5d). Thus, prior to the water flow simulations (Figures 5b and 5c), the HFE is located below the injection point and does not seem to migrate to the left or right of the cell. After the water table level variation, the reflection feature from the back of the cell is very similar to all the data acquired in the *y*-direction.

As the results were the same as in a previous experiment [*Orlando and Renzi*, 2013], no discussion is given here of the amplitude spectra of the trace giving overlapping information of the t.w.t. analysis.

In addition to the profile analyses, we also analyzed the three-dimensional features of the t.w.t of reflection from the back of the cell, taking into account only the *x*-direction profiles representative of the experiment.

The t.w.t. were performed by an automatic picking mode of the reflection from the back of the cell so as to link the variation between two travel times to the HFE position. The t.w.t. of the reflection from the back of the cell, acquired before HFE release (Figure 6), show an increase in times (up to 0.5 ns) in the middle of the cell, indicated by A in Figure 6. This anomaly is derived from the bulging of the cell, induced by the horizontal stresses of the host material inside the cell, as mentioned earlier. Anomaly A is detected in all the tests in the same position, though with small variations. The analysis of the test data (1–27) acquired over time was based on the residual time (C^n) (relation 1), which was obtained by subtracting from the t.w.t. of the reflection from the back of cell (A^n) of the nth test, the t.w.t. of the reflection of the data of test 1 (A^1) acquired before the release of HFE:

$$C_{i,j}^{n} = A_{i,j}^{n} - A_{i,j}^{1} \tag{1}$$

where A is the t.w.t of the reflection from the back of the cell, n the test number, j the profile number, i the trace number. In this way, the residual times depict the variation in time, i.e., the permittivity inside the cell over time.

At the top-left of Figure 7, there is a photo of the cell representative of the whole experiment. The pattern of the image does not change throughout the experiment. The blue color indicates the free HFE phase. The left of Figure 7 shows the residual times of representative tests of the experiment. The tests a, b, c monitor the t.w.t. variation before the water flow simulations at 0.30 (test 3), 92 (test 10), 190 (test 13) h after the

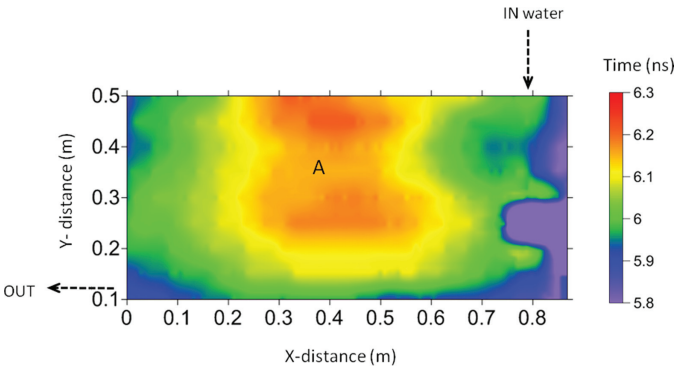

Figure 6. The t.w.t. of reflections from the back of the cell before the release of HFE (test 1).

release of HFE. Test 16 (Figure 7d) was surveyed 475 h after the release of HFE and several water flows, and finally test 27 (Figure 7e) monitors the cell after 155 days, following several water flows and a water table lowering to 35 cm from the bottom of the cell. In any case, the data of test 27 were collected in a saturated medium with the water level at the same position as in previous tests.

Half an hour after contaminant release (Figure 7a), the data show a decrease in t.w.t. (anomaly B at the left of Figure 7), which develops along the HFE flow with a minimum value at 0.35 cm from the bottom of the cell. Over time (Figures 7b and 7c) and also after several water flows (Figure 7d), the maps are quite similar. The minimum value of t.w.t. is about 0.36 ns. After the variation of the water table level (Figure 7e), the maps are arranged differently from the maps of the previous experiments. Sediments above the minimum level of the water table are characterized by lower residual t.w.t. values than those detected in sediments that remained saturated throughout the experiments. Moreover, along the flow of HFE, anomaly B disappears in correspondence with the sediments above the minimum level of the water table (dashed line in Figure 7e) but remains in the sediments below, though the amplitude is decreased in intensity. Considering these results, and those of the electrical parameters of the fluid described in the multiphase measures, it can be deduced that anomaly B is mainly due to the free phase of HFE; in fact, the anomaly remains in the same position after several water flow interventions and persists after the water table lowering/rising in sediments that remain saturated throughout the experiment.

In summary, the residual of t.w.t. shows: (i) the anomaly of the t.w.t linked to HFE remains in the same position throughout the experiment, with the minimum values located at 0.35 m from the bottom of the cell, showing that the water flows have probably removed only a small percentage of the contaminant; (ii) the main variations in the feature of the t.w.t distribution are induced by the water table variation. In fact, after the water table variation, the anomaly remains below the minimum level reached by the water (dashed line in Figure 7e).

3.3. Electrical Resistivity Measurements

The design of the measurement points and the effect of the cell boundary on apparent resistivity were analyzed on theoretical models. We calculated the theoretical apparent resistivity for a homogeneous medium, simulating media of different resistivity (from 10 to 100 Ωm) for cell dimension and array configuration similar to that used for the actual experiment. An analysis of the theoretical data shows that the apparent resistivity (collected with a minimum electrode offset of 7 cm in the *x*-direction, and electrodes 10 cm from the cell edge) is not sensitive to the edge of the cell.

Archie's [1942] law reveals that a linear relation links apparent resistivity to actual resistivity in a homogeneous permeable porous medium:

$$R = FR_w$$

where R is the resistivity of the medium, F the formation factor, and R_w the resistivity of water. This relation is not true in a nonhomogeneous medium.

Given the above considerations, it can be assumed that for measurements taken far from a site of free HFE phase the resistivity variation over time depends only on the resistivity variation of the water and the dissolved HFE phase, but when measured close to free phase HFE the variation depends on water and both the free and dissolved HFE phases. Therefore, the analysis of actual data was based on the apparent resistivity measured for the minimum electrode offset, as this describes the resistivity variation very well. To reduce

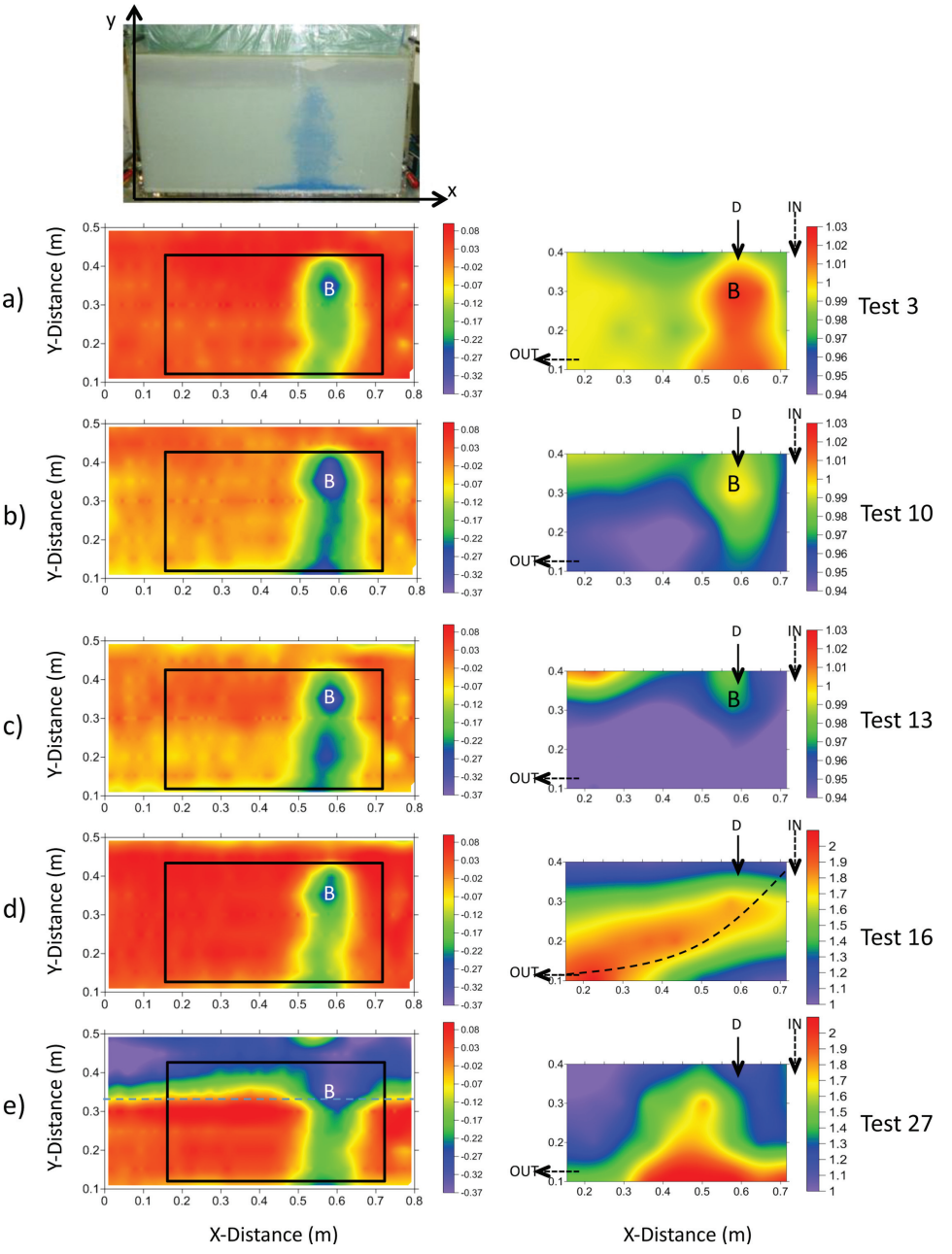

Figure 7. Comparison between some (left) GPR and (right) ERT data at the same time. Test acquired post DNAPL injection: (a) 30 min; (b) 92 h; (c) 190 h; (d) 475 h; (e) 155 days. ERT measures are normalized to data acquired before contaminant injection. GPR images show the variation in reflection time from the back of the cell. At the top-left, the cell image with the position (blue color) of free phase HFE. The scales are dimensioned in function of the data variability range. The GPR scale represents a residual two-way travel time (t.w.t.) and electrical resistivity in resistivity ratio (ρ_n/ρ_1).

and/or eliminate the effect of electrode-sediment coupling, we mapped the variation of the normalized resistivity inside the cell over time. The normalization was calculated through the relation (2):

$$C^n_{i,j} = R^n_{i,j}/R^1_{i,j} \tag{2}$$

where C^n is the normalized resistivity of test nth, R^n the apparent resistivity of test nth, R^1 the apparent resistivity of test 1, n the test number, j and i the x and y coordinates of the central position of the array, respectively.

The right side of Figure 7 shows the electrical resistivity measurements acquired in the same time as the GPR data.

The normalized resistivity of the tests, acquired before the water flow simulations (Figures 7a–7c), shows average values lower than those of test 1, while after water flow (Figures 7d and 7e) the maximum values are more than twice those of test 1. The average resistivity variation over time is not justified by the resistivity of the water injected into the cell or the temperature of the room as these did not vary substantially during the experiment. For the moment, not having any robust information, we can only advance same speculative hypothesis about the resistivity variation, for example, that the decrease in resistivity is due to unknown chemical reaction and/or to a biodegradation process similar to that shown by *Abdel et al*. [2006] for LNAPLs. The increase of the resistivity may be due to the flow of water that has replaced the fluid with clean water. The data acquired half an hour after the release of HFE (Figure 7a) show a resistive anomaly (B in Figure 7) lying underneath the point of HFE release, and 92 h after the release (Figure 7b) this anomaly has widened to extend along the HFE flow and into the upper part of the cell. The normalized resistive map of the data acquired 190 h after HFE release (Figure 7c) shows a pattern very similar to the earlier patterns though the resistive anomaly is, on average, slightly lower than previously. The increase of resistivity inside the cell, from the bottom to the top, indicates a resistivity variation of the fluid, which could also be due to volatile HFE components. The data collected after the water flows (Figure 7d) show an increased average resistivity throughout the cell and a resistive anomaly located along the water flow. The normalized resistivity data (Figure 7e) acquired 2 months after the HFE release, several water flows, and a lowering of the water table to 0.35 m, followed by a subsequent rising to the starting level, shows a noticeably changed distribution of resistivity within the cell with respect to the previous one. The minimum water level is indicated by the dotted black line in Figure 7e. The resistive anomaly is located in the lower-central part of the cell. On the basis of these results, we can advance the hypothesis that the resistive anomaly is mainly due to fluid, including water and both the dissolved and free phases of HFE, as the anomaly is wider than that detected by GPR and has high mobility within the cell over time.

The marked variation of resistivity distribution within the cell over time and the results obtained from the multiphase lab measures (Table 4) suggest that the electrical resistivity measurements are mainly sensitive to entire fluids. In fact, only the data, acquired 30 min after contaminant release (Figure 7a) show a resistive anomaly located along the contaminant flow. In all other tests, the resistivity distribution appears strictly related to the entire fluid.

3.4. Data Correlation

The integration of the results from the different methods allowed us to better detail the relation between geophysical anomalies and the physical parameters of different contaminant phases.

Data acquired 30 min after contaminant injection (Figure 7a) show a good overlap of normalized apparent resistivity and residual t.w.t. anomalies. Both methods detect anomalous values located in correspondence to HFE flow. The residual t.w.t maps of GPR data acquired 92 and 190 h after contaminant release (Figures 7b and 7c) are very similar to the previous test, while resistive anomaly B has widened and extends toward the top of the cell. At this stage, we observed a decrease in resistivity within the whole cell, which again increases after water flow activation, becoming more than twice the original one. This phenomenon is not easy to explain with our present knowledge, but we can hypothesize that the decrease in resistivity is due to a biodegradation process of the contaminant, like that described by *Abdel et al*., [2006] for LNAPL, or to a chemical process. Finally, after simulating the lowering/rising of the water table (Figure 7d), we observed a notable variation in the GPR and electrical resistivity maps with respect to the previous data. At this stage, the data show a resistive anomaly located in the mid to lower part of the cell, and anomalous residual times in the upper part of the cell and below the contaminant release. This led to the hypothesis that the lowering of the water is the main cause of downward DNAPL migration as it appears to be not totally removed from the sediments, which remained saturated throughout the experiment.

Comparison of the electrical resistivity and residual t.w.t of GPR data shows that both kinds of data are sensitive, in different ways, to free and dissolved HFE phases. GPR seems to be sensitive mainly to the free phase, and electrical resistivity to all fluids. These results were validated also by the measures of electrical resistivity and permittivity of single fluids and their mixtures. We observed that the chemical phenomena

occurring in the lab experiment are very complex, and are not at all easily explicable at this stage. For this reason, the resistivity anomalies are more difficult to interpret than the permittivity ones as permittivity is mainly influenced by free phase HFE, and resistivity by all the fluids present.

4. Conclusions

The study was based on the monitoring of electrical resistivity and permittivity by using of electrical resistivity and GPR data. We showed that such measurements are sensitive, in different ways, to the different fluids present in a HFE contaminated site and that not always the changes in the observed physical parameters can be justified with the knowledge that we currently have on the chemical process that can occur in such a context, albeit simplified as the one considered in the experiment.

The measurements of the electrical permittivity and the resistivity of free phase HFE have shown that such HFE is characterized by a lower electrical permittivity and higher resistivity than water. Indeed, HFE in water is present as dissolved and free phases. The dissolved phase induces small variations in the electrical permittivity of the multiphases of contaminated water, while the entire fluid strongly influences resistivity. After simulating the lowering/rising of the water table, the resistivity and residual t.w.t. distribution inside the cell were very varied. This led to the hypothesis that the lowering/rising of the water table seems to be more effective than water flow in the downward movement of HFE, as demonstrated by tests d and e of Figure 7. In fact, using electrical resistivity measurements, we found that immediately after water flow the resistive anomaly is located in the same position as the water flow. In conclusion, the combining of different electromagnetic methods makes it possible to better appreciate the behavior of a complex multiphase system. Furthermore, the study has shown that the t.w.t. of reflection behind the contaminant can be useful in detecting the free HFE phase, and electrical resistivity is more sensitive to the entire fluid. Finally, the lab experiments led to the conclusion that HFE is not easily removed from a saturated medium as its free phase remains trapped within the pores and it moves very slowly downward, even after several water flows. Over a long period of time, the free phase might decompose into the dissolved one, thus facilitating its removal. Water flow contributes to the removal of the dissolved phase over time, as demonstrated by the electrical resistivity measurements that show that immediately after the flow of water, the resistive anomalies are located in the middle of the cell, in the same position as the water flow.

The results of the described experiment represent a preliminary step toward a more in-depth study of the different capabilities of electromagnetic methods for the detection and monitoring of different phases of HFE in a saturated medium. The study, as often occur in scientific research, leaves open some issues, which can only be resolved by conducting further experiments in order to analyze the chemical and biochemical processes that cause some changes in the physical characteristics measured during this study that are not currently supported by robust scientific analysis.

In the future, it will be important to analyze the complex chemical process that occurs in a contaminated medium, and to gain an understanding of how it interacts with the physical parameters measured using geophysical methods.

Acknowledgment
The research was funded with both academic and private funds.

References

Abdel, G. Z., L. D. Slater, and E. A. Atekwana (2006), Induced-polarization measurements on unconsolidated sediments from a site of active hydrocarbon biodegradation, *Geophysics*, *71*(2), H13–H24.

Ajo-Franklin, J. B., J. T. Geller, and J. M. Harris (2004), The dielectric properties of granular media saturated with DNAPL/water mixtures, *Geophys. Res. Lett.*, *31*, L17501, doi:10.1029/2004GL020672.

Archie, G. E. (1942), The electrical resistivity log as an aid in determining some reservoir characteristic, *Pet. Trans. AIME*, *142*, 54–62.

Bano, M., O. Loeffler, and G. Jean-François (2009), Ground penetrating radar imaging and time-domain modelling of the infiltration of diesel fuel in a sandbox experiment, *Geoscience*, *341*, 846–858.

Bradford, S. A., K. M. Rathfelder, L. Lang, and L. M. Abriola (2003), Entrapment and dissolution of DNAPLs in heterogeneous porous media, *J. Contam. Hydrol.*, *67*, 133–157.

Brewster, M., and P. Annan (1994), Ground-penetrating radar monitoring of a controlled DNAPL release: 200 MHz radar, *Geophysics*, *59*, 1211–1221.

Brusseau, M. L., N. T. Nelson, Z. Zhang, J. E. Blue, J. Rohrer, and T. Allen (2007), Source-zone characterization of a chlorinated-solvent contaminated Superfund site in Tucson, AZ, *J. Contam. Hydrol.*, *90*(1–2), 21–40.

Cardarelli, E., and G. Di Filippo (2009), Electrical resistivity and induced polarization tomography in identifying the plume of chlorinated hydrocarbons in sedimentary formation: A case study in Rho (Milan-Italy), *Waste Manage. Res.*, *27*(6), 595–602.

Cassidy, N. J. (2007), Evaluating LNAPL contamination using GPR signal attenuation analysis and dielectric property measurements: Practical implications for hydrological studies, *J. Contam. Hydrol.*, *94*, 49–75.
Chambers, J. E., R. D. Ogilvy, and P. I. Meldrum (2004), Non-invasive monitoring of DNAPL migration through a saturated porous medium using electrical impedance tomography, *J. Contam. Hydrol.*, *68*(1-2), 1–22.
Chambers, J. E., P. B. Wilkinson, G. P. Wealthall, M. H. Loke, R. Dearden, R. Wilson, D. Allen, and R. D. Ogilvy (2010), Hydrogeophysical imaging of deposit heterogeneity and groundwater chemistry changes during DNAPL source zone bioremediation, *J. Contam. Hydrol.*, *118*, 43–61.
Daily, W., and A. Ramirez (1995), Electrical resistance tomography during in-situ trichloroethylene remediation at the Savannah River Site, *J. Appl. Geophys.*, *33*(4), 239–249.
Fure, A. D., J. W. Jawitz, and M. D. Annable (2006), DNAPL source depletion: Linking architecture and flux response, *J. Contam. Hydrol.*, *85*(3–4), 118–140.
Goes, B. J. M., and J. A. C. Meekes (2004), An effective electrode configuration for the detection of DNAPLs with electrical resistivity tomography, *J. Environ. Eng. Geophys.*, *9*(3), 127–141.
Hwang, Y. K., A. L. Endres, S. Piggott, and B. Parker (2008), Long-term ground penetrating radar monitoring a small volume DNAPL release in a natural groundwater flow field, *J. Contam. Hydrol.*, *97*, 1–12.
Illangasekare, T. H., J. L. Ramsey, K. H. Jensen, and M. Butts (1995), Experimental study of movement and distribution of dense organic contaminants in heterogeneous aquifers: An experimental study, *J. Contam. Hydrol.*, *20*(1), 1–25.
Isalou, M., B. E. Sleep, and S. N. Liss (1998), Biodegradation of high concentrations of tetrachloroethene in a continuous flow column system, *Environ. Sci. Technol.*, *32*(22), 3579–3585.
Johnson, R. H., and E. P. Poeter (2005), Interpreting DNAPL saturations in a laboratory-scale injection using one- and two-dimensional modeling of GPR data, *Ground Water Monit. Rem.*, *25*(1), 159–169.
Kamon, M., K. Endo, and T. Katsumi (2004), Two-dimensional DNAPL migration affected by groundwater flow in unconfined aquifer, *J. Hazard. Mater.*, *110*, 1–12.
Kavanaugh, M. C., et al. (2003), *The DNAPL Remediation Challenge: Is There a Case for Source Depletion?* U.S. Environ. Prot. Agency, Washington, D. C.
Kueper, B. H., and E. O. Frind (1991), Two-phase flow in heterogeneous porous media: 1. Model development, *Water Resour. Res.*, *27*, 1049–1057.
Mazác, O., L. Benes, I. Landa, and A. Maskova (1990), Determination of the extent of oil contamination in groundwater by geoelectricalmethods, in *Geotechnical and Environmental Geophysics*, vol. II, edited by S. H. Ward, pp. 107–112, Soc. of Explor. Geophys., Tulsa, Okla.
Morris, C. G. (1992), *Dictionary of Science and Technology*, Academic press, San Diego, Calif.
Nambi, I. M., and S. E. Powers (2003), Mass transfer correlations for nonaqueous phase liquid dissolution from regions with high initial saturations, *Water Resour. Res.*, *39*, 1030, doi:10.1029/2001WR000667.
Newmark, R. L., W. D. Daily, K. R. Kyle, and A. L. Ramirez (1998), Monitoring DNAPL pumping using integrated geophysical techniques, *J. Environ. Eng. Geophys.*, *3*(1), 7–13.
Olhoeft, G. R. (1992), Geophysical detection of hydrocarbon and organic chemical contaminats, in SAGEEP Proceedings, pp 587–595, Oakbrook, Ill, doi:10.4133/1.2921962.
Orlando, L., and B. Renzi (2013), Time-lapse monitoring of DNAPL in a controlled cell, *Near Surface Geophys.*, *11*, 129–142.
Page, J. W. E., K. Soga, and T. Illangasekare (2007), The significance of heterogeneity on mass flux from DNAPL source zones: An experimental investigation, *J. Contam. Hydrol.*, *94*, 215–234.
Parker, J. C., and E. Park (2004), Modeling field-scale dense non-aqueous phase liquid dissolution kinetics in heterogeneous aquifers, *Water Resour. Res.*, *40*, W05109, doi:10.1029/2003WR002807.
Powers, S. E., I. M. Nambi, and G. W. Curry (1998), Non-aqueous phase liquid dissolution in heterogeneous systems: Mechanisms and a local equilibrium modeling approach, *Water Resour. Res.*, *34*(12), 3292–3302.
Saba, T., and T. H. Illangasekare (2000), Effect of groundwater flow dimensionality on mass transfer from entrapped non-aqueous phase liquid contaminants, *Water Resour. Res.*, *36*(4), 971–979.
Schwille, F. (1988), *Dense Chlorinated Solvents in Porous and Fractured Media*, 146 pp., Lewis Publ., Chelsea, Mich.
US EPA (Environmental Protection Agency) (2004), *Site Characterization Technologies for DNAPL Investigations*, U.S. Environ. Prot. Agency, Washington, D. C.
Weller, A., M. Gruhne, M. Seichter, and F. D. Börner (1996), Monitoring hydraulic experiments by complex conductivity tomography, *Eur. J. Eng. Geophys.*, *1*, 209–228.